Discover

Research

An investigation on the structural and optical properties of mercaptosuccinic acid capped cadmium telluride quantum dots

Dibya Jyoti Borah[1] · D. Saikia[2] · A. Das[2] · P. K. Saikia[2] · A. T. T. Mostako[1]

Abstract

In this work, a sonication induced modified wet chemical approach is adopted to synthesize highly luminescent and water soluble cadmium telluride (CdTe) quantum dots (QDs). The morphology, size, crystal structural, and optical properties of CdTe QDs are investigated for different refluxing time (1–4 h). The refluxing time-dependent optical constants viz. band gap energy and Urbach energy of the QDs are estimated from UV–Visible absorption spectra. The optical band gap energy decreased from ~ 2.12 to 1.92 eV and the Urbach energy increased from ~ 361 to 487 meV, with the increase in refluxing time. CdTe QDs are found to be uniform in size. The average size of the QDs estimated from the High Resolution Transmission Electron Microscope image analysis is about 5.8 and 8.2 nm for refluxing times 1 and 4 h, respectively. The growth mechanism of the QDs as a function of refluxing time has also been discussed. The fluorescence spectra of the QDs, revealed emission peaks having wavelength from ~ 534 to 585 nm, under the excitation wavelength of 320 nm. The fluorescence emission peaks showed a bathochromic shift with increasing refluxing time. CdTe QDs also exhibit excitation-dependent fluorescence behaviour. Two crystalline phases of the CdTe QDs, namely hexagonal and cubic are confirmed from the High Resolution Transmission Electron Microscope images and Selected Area Electron Diffraction patterns analysis. The phase transformation from hexagonal to cubic is successfully achieved by tuning the refluxing time from 1 to 4 h.

Keywords CdTe QDs · Sonication · Wet chemical · Refluxing time · Tunable fluorescence · Phase transformation

1 Introduction

Over the past few decades, the nanostructures of II-VI semiconductor compounds have gained immense research attention because of their unique and attractive properties viz. easy tunability of band gap, highly fluorescent nature, high carrier concentration, good transmission ability, and good chemical stability [1, 2]. Among these compounds, the binary semiconductor compound cadmium telluride (CdTe) is extensively studied because of its high absorption coefficient ~ 10^5 cm^{-1}, high electron mobility, direct band gap energy in the range of ~ 1.4–1.5 eV, large Bohr exciton radius of 7.3 nm, and high work function [1, 3, 4]. Moreover, CdTe possesses different crystalline phases viz. cubic, tetragonal, orthorhombic, and hexagonal [5, 6]. Among these crystalline phases, cubic is found to be the most stable phase [3, 7]. Upon heat treatment, the metastable hexagonal phase of CdTe transforms to its highly stable cubic phase [3, 7]. Spray pyrolysis deposited CdTe thin film transforms from its hexagonal to cubic phase under the influence of ion beam

✉ Dibya Jyoti Borah, jyotidibya2015@gmail.com; ✉ A. T. T. Mostako, mostako@dibru.ac.in | ¹Material Science Laboratory, Department of Physics, Dibrugarh University, Dibrugarh, Assam 786004, India. ²Thin Film Laboratory, Department of Physics, Dibrugarh University, Dibrugarh, Assam 786004, India.

Springer

irradiation [8]. In contrast, the cubic to hexagonal crystalline phase transition produced by the oxygen incorporation into the non-oxygenated radio frequency sputtered cubic CdTe thin film is reported by Arizpe-Chavez et al. [9]. Due to these fascinating properties, CdTe shows excellent photovoltaic characteristics and is used as a potential sensitizer in third generation solar cells [1, 2, 4].

Quantum dots (QDs) exhibit size-dependent optical, structural, and electronic properties owing to the quantum confinement effect [10, 11]. Over the recent years, CdTe QDs have received remarkable research attention because of their tunable band gap, high fluorescence efficiency, and high quantum yield [1, 2, 12]. They can be made to show tunable photo-luminescent properties in the visible spectrum (~ 500–750 nm) by controlling their particle size [13, 14]. Moreover, a single excitation wavelength of light can simultaneously excite all colours of CdTe QDs [1, 13, 15]. Due to these exceptional properties, CdTe QDs are attractive for applications in fingerprint development [13], bio-imaging [16], and metal-ion sensing [17].

Various methods have been employed for the synthesis of CdTe QDs [18–22]. Ananthakumar et al. [18] prepared mercaptopropionic acid (MPA) capped CdTe QDs using one-pot approach. They studied the size-dependent up-conversion photoluminescence (PL) of the as prepared CdTe QDs as a function of refluxing time [18]. Using a simple modified one-pot method, Ca et al. [19] prepared Ni-doped CdSeTe QDs and investigated the Ni-doping concentration-dependent optical band gap energy, PL intensity, and the quantum yield of the QDs. Gold nanoparticles coated with a thioglycolic acid (TGA) capped CdTe QDs synthesized by a chemical based method, and studied their application as a theranostic agent in nanotechnology-based cancer detection and therapy [20]. Nideep et al. [21] reported the synthesis of mercaptosuccinic acid (MSA) capped CdTe QDs via colloidal chemical route, for pH sensing applications. Yuan et al. [22] employed CdTe QDs capped with glutathione (GSH) and investigated the influence of QDs sizes for sensitive detection of glucose. In the aforementioned methods, most of the researchers have used MPA, TGA, and GSH capping agents during the synthesis of CdTe QDs. Instead, to limit the size of QDs, MSA is used as a capping agent in the present work. Because, the molecular structure of MSA consists of both MPA- and TGA- like molecular structure, which possesses the combination of single coordination and double coordination similar to MPA and TGA, respectively [23]. This leads to faster growth rate of MSA capped CdTe QDs during the synthesis process as well as Ostwald ripening growth process as compared to that of TGA or MPA capped CdTe QDs [23]. Moreover, Ying et al. [24] and Parani et al. [25] reported that the molecular structure of MSA, with pK_{COOH} values of 3.30 and 4.94, possesses both the properties of MPA and TGA, with pK_{COOH} values of 4.32 and 3.53, respectively. MSA can stabilize CdTe QDs in both acidic and alkaline media, while the capping agents MPA and TGA can stabilize the QDs only in alkaline medium [24, 25]. The structure of MSA consists of two carbonyl groups, which provide better stability as compared to that of TGA and MPA capping agents which consist of thiol groups in their molecular structures [24, 25]. This leads to improve the fluorescence efficiency as well as plays a beneficial role in the imaging of cancer cells [24, 25].

In this present work, MSA capped CdTe QDs were synthesized by adopting a sonication induced modified wet chemical approach. This is a combination of ultrasonication and wet chemical approach for the synthesis of QDs. In this modified method, sonication is performed, where the induced ultrasonic waves fragment the larger particles into smaller ones which leads to the formation of well-dispersed QDs in the solution. In this approach, the synthesis parameters viz. pH of the solution, concentration of reactants, refluxing time, and temperature can be controlled to synthesize desired particle size and crystalline phase of the QDs. In addition to that, in this sonication induced modified wet chemical approach, additional sonication parameters viz. sonication frequency, sonication bath temperature, and sonication duration can be varied for the synthesis of tunable size and crystalline phase of the QDs. Keeping these in mind, at constant synthesis parameters viz. pH of the solution, refluxing temperature, sonication frequency, sonication bath temperature, and sonication duration; the effect of refluxing time on the crystal structural and optical properties of MSA capped CdTe QDs are investigated in the present work.

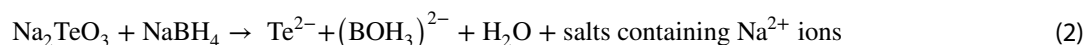## 2 Experimental details

2.1 Materials and reagents

The chemicals used during the sonication induced wet chemical approach were analytical grade Cadmium Chloride [$CdCl_2$] (Merck, 99%), MSA (Loba Chemie, 98%), Sodium Tellurite [Na_2TeO_3] (Loba Chemie, 98%), Sodium Borohydride [$NaBH_4$] (Merck, 98%), Citric acid [$C_6H_8O_7$], Sodium Hydroxide [NaOH], and Borax powder. Deionized water was used throughout this experiment.

2.2 Synthesis of CdTe QDs

In the present work, CdTe QDs were synthesized by a sonication induced wet chemical approach. Firstly, a solution containing 20 mL of 0.75 mM Na_2TeO_3, 20 mL of 3 mM $CdCl_2$, and 20 mL of 9 mM MSA was prepared and stirred to get a homogeneous mixture. This mixture was then added to a buffer solution. The buffer solution was prepared by using 10 mL of 15 mM Borax and 10 mL of 15 mM Citric acid. The whole solution was stirred properly using a magnetic stirrer for 15 min and finally kept in a three-neck round bottom flask. The pH of the solution was maintained at ~6 by adding aqueous NaOH and then 40 mg of $NaBH_4$ was added to it. Finally, the solution mixture was refluxed at ~100 °C for 1 h. After refluxing, a light brown colour solution was obtained. The brown coloured sample solution was sonicated with a frequency ~50 Hz at sonication bath temperature of 45 °C for 30 min, for the formation of well-dispersed particles in the solution. The experiment was repeated by changing the refluxing time from 1 to 4 h with an interval of 1 h, four samples were prepared. The samples were coded as S_1, S_2, S_3, and S_4, respectively. The expected reaction mechanism for the synthesis of the CdTe QDs is enumerated as follows [1, 26];

$$CdCl_2 + H_2O + MSA \ \rightarrow \ CdX + 2HCl + O \ (X = MSA) \tag{1}$$
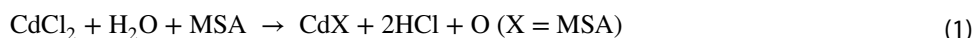
Tellurium ions are released according to the following reaction,

$$Na_2TeO_3 + NaBH_4 \rightarrow \ Te^{2-} + (BOH_3)^{2-} + H_2O + salts \ containing \ Na^{2+} \ ions \tag{2}$$

Finally, the formation of CdTe occurs in accordance with the following reaction,

$$CdX + Te^{2-} \rightarrow \ CdTe + X \tag{3}$$

The average size and morphology of the CdTe particles were analysed by using a Transmission Electron Microscope (TEM), Model: JEOL JEM-2100. High Resolution Transmission Electron Microscope (HRTEM) images and Selected Area Electron Diffraction (SAED) patterns of the samples were analysed to evaluate the crystallographic orientation of the CdTe particles. HRTEM images, and SAED patterns were analysed by using Image J software. For the investigation of optical constants, UV–Visible absorption spectra of the samples were recorded by a UV–Visible Spectrophotometer, Model: Shimadzu UV–Vis 2600, in the wavelength range 200–1100 nm with a spectral resolution of 1 nm. Fluorescence (FL) spectra of the samples were recorded by using a Spectrophotometer, Model: Horiba Jovi Yvon Fluoromax 4P. The Fourier transform infrared (FTIR) spectrum of the sample was recorded by Bruker Alpha II Compact FTIR Spectrometer, in the wavenumber range 500–4000 cm^{-1}, to confirm the capping of MSA molecules over the CdTe particles.

3 Results and discussion

3.1 Crystal structural analysis of CdTe QDs

TEM image analysis was performed to investigate the average size and crystal structure of the synthesized MSA capped CdTe particles. TEM images of the MSA capped CdTe particles synthesized at refluxing times 1 and 4 h are shown in Fig. 1a, b, respectively. Both the TEM images showed the cluster of nanosized particles of sizes less than ~10 nm. Therefore, better confirmation of shape as well as individual size of the particles, HRTEM diagnostics is performed. The magnified HRTEM images of the samples: S_1 and S_4 are shown in Fig. 2a, b respectively, while the insets shows the particle size distribution histograms. The average size among twenty-five particles obtained from the distribution histograms for the samples: S_1 and S_4 are ~5.8 and 8.2 nm, respectively. Moreover, the HRTEM image along with the magnified areas of two arbitrarily selected QDs of sample S_1 are shown in Fig. 3a and its insets, respectively. The crystalline lattice fringes with interplanar spacings of ~0.25 and 0.30 nm correspond to the (013) and (102) lattice planes of hexagonal phase of CdTe, respectively (JCPDS card no. 82-0474). The corresponding SAED pattern of the sample S_1, Fig. 3b, displays distinguishable diffraction rings which can be well indexed to the (213) and (013) lattice planes of CdTe hexagonal phase. Similarly, for sample S_4, HRTEM image and the magnified areas of two QDs selected arbitrarily, are shown in Fig. 3c and its insets, respectively. Two sets of orthogonal lattice fringes with an interplanar spacing of ~0.22 and 0.37 nm correspond to the (220) and (111) lattice planes of cubic phase of CdTe, respectively (JCPDS card no. 15-0770). Bright diffraction spots observed in the corresponding SAED pattern, Fig. 3d, could be well indexed to the (220) and (111) lattice planes of cubic phase

Fig. 1 TEM images of CdTe particles for the samples, **a** S_1 and **b** S_4, respectively
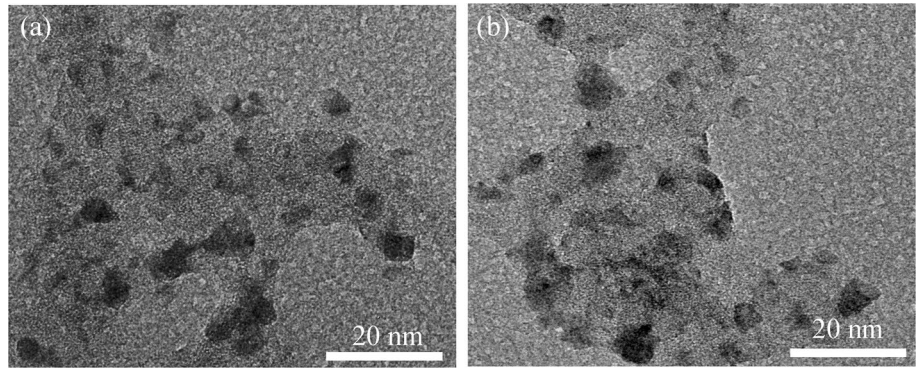

Fig. 2 HRTEM images (inset particle size distribution histograms) of CdTe particles for the samples, **a** S_1 and **b** S_4, respectively
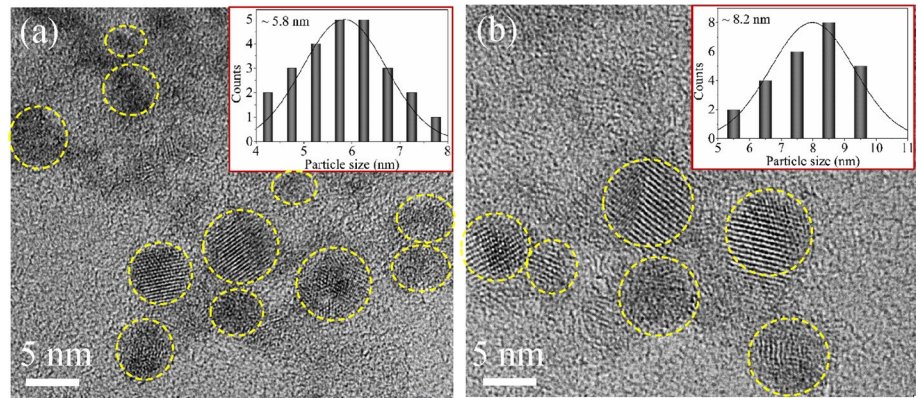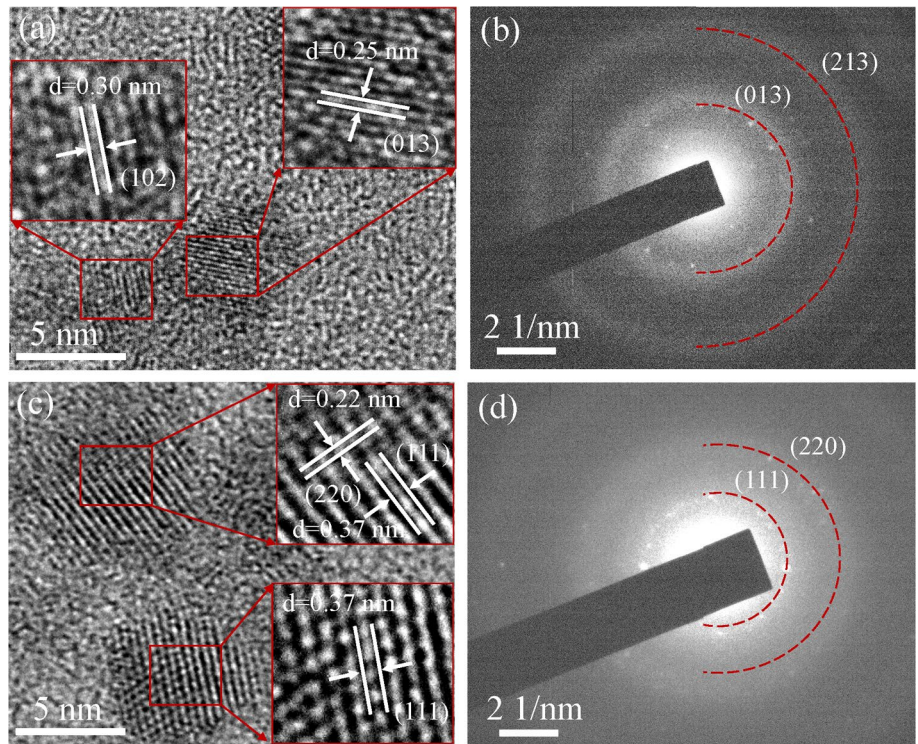

Fig. 3 HRTEM image and corresponding SAED pattern of the samples, S_1 (**a** and **b**) and S_4 (**c** and **d**), respectively

of CdTe. The average particle sizes and interplanar spacings, along with the crystal planes estimated from the HRTEM images and SAED patterns, respectively, for the samples: S_1 and S_4 are listed in Table 1. The average size of the particles are found to increase with the refluxing time. Lower refluxing time favours the formation of few number of CdTe monomers in the reaction solution. Therefore, the inter-particle spacing is higher for which there is less mass transfer in the reaction medium. Higher refluxing time maintained the reaction kinetics in the sample solutions for longer duration of time, which is favourable for the formation of more number of CdTe particles. This leads to the decrease in inter-particle spacing and increase in mass transfer in the solution medium along with higher growth rate of the CdTe QDs. In the present work, refluxing was performed on all the samples at ~100 °C for different durations. At lower refluxing time, there is a minimum thermal energy gain by the reactive ions in the sample solution during the reaction kinematics, which supports the formation of metastable hexagonal phase of CdTe QDs. At the longer refluxing time, due to increase in the mass transfer in the reaction medium, thermal energy gain by reactive ions is higher, leading to greater surface mobility over the QDs. Since, the stacking fault energy differences for the cubic and hexagonal phase has been found to be only 11 meV per atom for CdTe, indicating the free energy difference between the cubic and hexagonal crystal lattice is small [7]. Therefore, thermal energy achieved by the reactive ions on the surface of the QDs at longer refluxing time allows an activation of metastable hexagonal phase to lower energy stable cubic phase.

3.2 Optical properties of CdTe QDs

The UV–Visible absorption spectra, in wavelength range ~350–800 nm, of MSA capped CdTe QDs samples: S_1-S_4, are shown in Fig. 4a. The maximum absorbance of the samples appeared in the wavelength range of ~350–359 nm. A small and broad absorption peaks are observed at ~490–521 nm for the samples: S_1-S_4, respectively. These absorption peaks are attributed to the occurrence of the first excitonic transition ($1s_h \rightarrow 1s_e$) between the allowed energy levels [14]. These first absorption excitonic peaks are not clearly visible in the absorption spectra. This is attributed to the longer period of refluxing which might lead to the Ostwald ripening [7]. The absorption excitonic peak appeared at ~490 nm for the sample S_1, is shifted to ~521 nm with the increase in refluxing time. This bathochromic shift of absorption peak with the refluxing time indicates the increase in the size of CdTe QDs as a consequence of quantum confinement [14]. The absorption peak intensity of the QDs in the sample is observed to increase with the refluxing time. This is due to the presence of more number of CdTe monomers at higher refluxing times. No distinct precipitation was observed in the brownish suspension solution of the CdTe QDs, even after several weeks of storage. The optical band gaps (E_g) of the QDs are estimated by using the Tauc's Eq. (4) [12, 27],

$$\alpha h\upsilon = B(h\upsilon - E_g)^m \qquad (4)$$

where, B is the Tauc's slope, $h\upsilon$ is the photon energy, and α is the absorption coefficient and m is the transition probability. For a material with a direct band gap, m takes a value of ½ for allowed transitions [12]. The $(\alpha h\upsilon)^2$ versus $h\upsilon$ plots for the samples: S_1–S_4, are depicted in the Fig. 4b. The values of the optical band gap of the samples: S_1–S_4, as estimated from their respective Tauc's plots, are ~2.12, 2.07, 2.01, and 1.92 eV, respectively, and are accordingly listed in Table. 1. The estimated values of band gap are quite large as compared to that of bulk CdTe band gap ~1.4–1.5 eV [3]. This again indicates the formation of CdTe QDs. Moreover, the values of the optical band gap are found to decrease from ~2.12 to 1.92 eV with the increase of refluxing time from 1 to 4 h. A similar trend of optical band gap for CdTe QDs with increasing refluxing time is also observed in the range ~3.49–3.15 eV, by Gharibshahi et al. [12]. This change in optical band gap is attributed to the increase in the size of QDs as confirmed by HRTEM image analysis. The average particle sizes of CdTe QDs were determined by first excitonic absorption peaks of wavelength of UV–Visible absorption spectra by using Brus effective mass approximation Eq. (5) [28, 29],

$$E_g = E_{g(bulk)} + \frac{h^2}{8R^2}\left(\frac{1}{m_e^*} + \frac{1}{m_h^*}\right) - \frac{1.786e^2}{4\pi\varepsilon_o\varepsilon_r R} \qquad (5)$$

where, $E_{g(bulk)}$ is the band gap of bulk CdTe, R is the radius of particle, h is the Planck's constant, m_e^* is the effective mass of excited electron, m_h^* is the effective mass of hole, e is the charge of electron, ε_o is the permittivity of vacuum, ε_r is the dielectric constant of CdTe. Due to the high value of dielectric constant of CdTe, the third term in Eq. (5) can be neglected. The estimated average particle sizes are ~5.6, 6.1, 6.4, and 7.2 nm for the samples: S_1-S_4, respectively, and are accordingly listed in Table 1. These average particle sizes are well consistent with the average sizes obtained from HRTEM observation.

Table 1 Estimated optical and crystal structural parameters of CdTe QDs along with the sample codes

Sample code	Refluxing time (hr)	Band gap energy, E_g (eV)	Urbach energy, E_u (meV)	Average particle size from Brus Eq. (nm)	Average particle size from HRTEM (nm)	Inter planar spacing, d (nm)	(hkl) planes	Phase assignment
S_1	1	~2.12	361	~5.6	~5.8	0.25	(013)	Hexagonal
						0.30	(102)	Hexagonal
S_2	2	~2.07	390	~6.1	–	–	–	–
S_3	3	~2.01	421	~6.4	–	–	–	–
S_4	4	~1.92	487	~7.2	~8.2	0.22	(220)	Cubic
						0.37	(111)	Cubic

Fig. 4 **a** UV–Visible absorption spectra and **b** plot of $(\alpha h\upsilon)^2$ versus $h\upsilon$ of CdTe QDs for the samples: S_1–S_4, respectively.
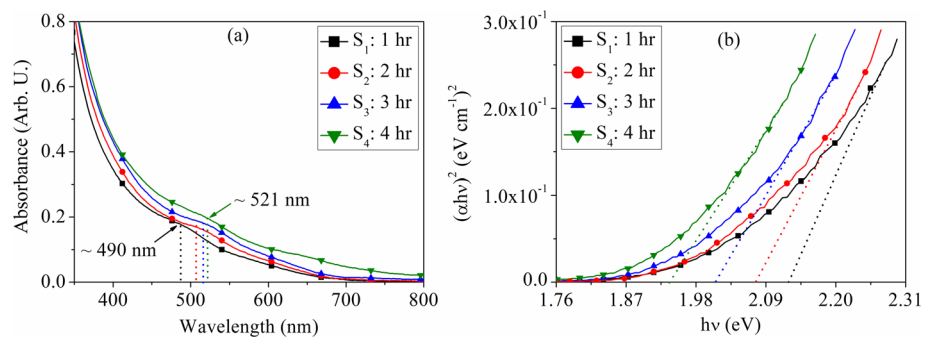
The width of the optical absorption tail of the localized states in the forbidden gap gives a measure of the Urbach energy, and is associated with the structural disorder or defects in a crystalline material. The spectral dependence of absorption coefficient and photon energy follows the empirical Urbach rule, given by Eq. (6) [30],

$$\alpha = \alpha_o \exp(h\upsilon/E_u) \qquad (6)$$

where α_o is a constant and E_u is the Urbach energy. A straight line equation is obtained by taking logarithm on both sides of Eq. (6), as given by Eq. (7) [30],

$$\ln\alpha = \ln\alpha_o + (h\upsilon/E_u) \qquad (7)$$

The plots of $\ln(\alpha)$ versus $h\upsilon$ for the samples: S_1–S_4, are shown in Fig. 5. The reciprocal of the slope of the fitted straight line in $\ln(\alpha)$ versus $h\upsilon$ plots gives the values of the Urbach energy, which are accordingly listed in Table. 1. Figure 6 depicts the changes in the Urbach energy and the band gap energy of the samples: S_1–S_4, with the refluxing time. The values of Urbach energy.are found to increase with the increase in refluxing time. This is attributed to the widening of the localized band states; as a consequence, an increase in defect density states near the exponential absorption edge is observed [11, 31, 32].

The FL images of the CdTe QDs samples: S_1-S_4 under UV light irradiation at 365 nm are shown in Fig. 7a. The FL colours of the solution of CdTe QDs change from green to orange-red with the increase of refluxing time. This indicates the possibility of the variation of the size of the CdTe QDs as function of refluxing time. In order to further study the optical properties.of the MSA capped CdTe QDs, FL spectra of the samples were recorded under an excitation

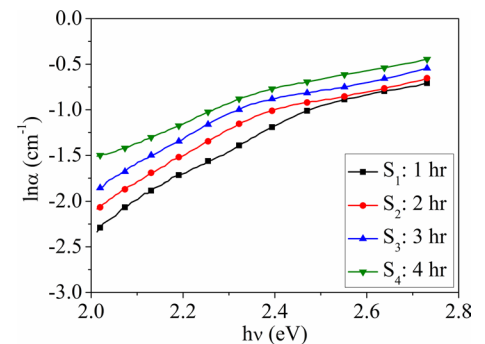**Fig. 5** The plot of $\ln\alpha$ versus $h\upsilon$ of CdTe QDs for the samples: S_1–S_4

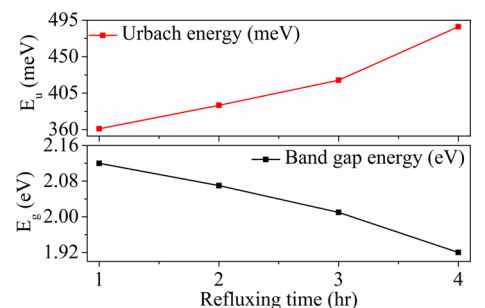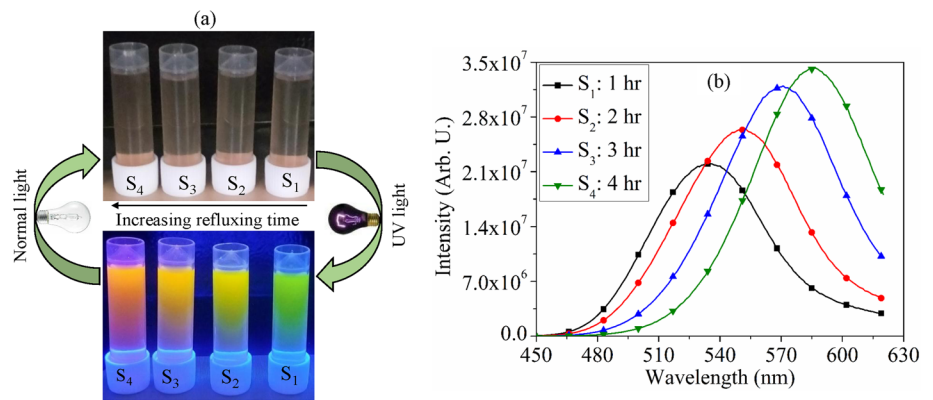**Fig. 6** The E_g and E_u variation with refluxing time for the samples: S_1–S_4

Fig. 7 a Photographs of the CdTe QDs samples: S_1-S_4 are captured under normal light and irradiated with UV light at 365 nm, **b** FL spectra of the samples: S_1-S_4 with an excitation wavelength 320 nm, respectively

wavelength of ~ 320 nm as is shown in Fig. 7b. Strong FL emission peak observed at ~ 534, 550, 570, and 585 nm wavelengths for the samples: S_1-S_4, respectively. This distinct FL emission peak in all four samples can be ascribed to the $1s_h \rightarrow 1s_e$ exciton recombination due to an intense exciton-phonon coupling [14]. It is clearly observed from Figs. 4a and 7b that stokes shifts are found to be ~ 44, 47, 55, and 64 nm for the samples: S_1–S_4, respectively. This is due to the presence of emissive trap states on the surface of MSA capped CdTe QDs and phonon assisted thermodynamic lattice vibration [1, 2, 33]. Similar to the absorption spectra, a bathochromic shift of FL emission peak is observed with the increase of refluxing time. This shift of the FL emission peaks indicates the increase of size of the QDs. This is due to the presence of a relatively higher number of CdTe monomers, and their inter-coupling due to Ostwald ripening [1, 13]. There is also an increase in the intensity of the FL emission peak with the increase in refluxing time. This can be attributed to higher FL quantum yield and the formation of better crystallinity of the CdTe QDs at longer durations of refluxing time [1]. Figure 8 shows the excitation-dependent FL spectrum of CdTe QDs for the sample S_1. The FL emission peaks bathochromically shifted from ~ 541 to 603 nm for the sample S_1 with an increase in the excitation wavelength from 340 to 375 nm. The FL intensity was observed to change with excitation wavelengths. This is because of the inhomogeneity of chemical components and polydispersity of the lateral sizes, which is again in consistent with HRTEM observation [34, 35]. This phenomenon is mostly likely due to the distribution of emissive trap sites on the surface of CdTe QDs and quantum confinement effect [34, 35]. Similar observation for molybdenum trioxide (MoO_3) QDs is reported in our previous research works [10, 11].

The FTIR spectrum of the functional groups of the MSA capped CdTe QDs for the sample S_1 is depicted in Fig. 9. A broad absorption peak at ~ 3310 cm^{-1} is attributed to the O–H stretching vibrations of the water molecules of the aqueous solution [2, 36]. A weak absorption peak associated with C = O vibrations was observed at 2123 cm^{-1} [37]. The stretching vibration band of −COOH is found at ~ 1675 cm^{-1}, which occurs due to the asymmetric vibrations of COO^- ions present in MSA capped CdTe QDs [36]. The two weak absorption peaks located at ~ 678 and 671 cm^{-1} in MSA capped CdTe QDs are attributed to the presence of C-S vibrations of MSA [2].

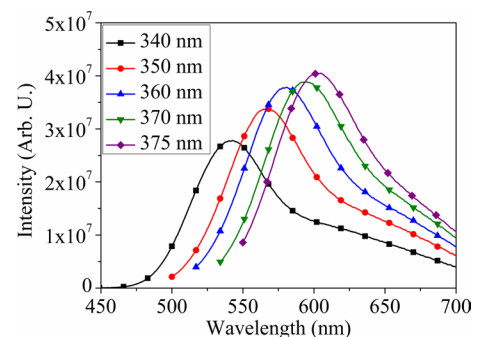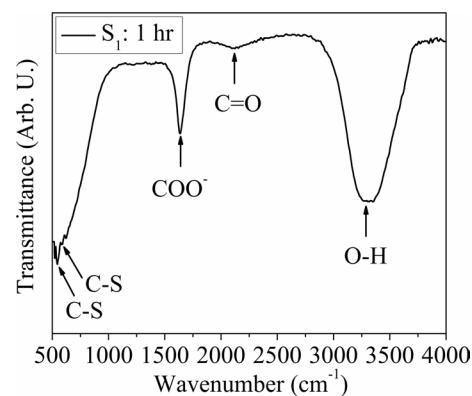**Fig. 8** Excitation-dependent FL spectrum of CdTe QDs for the sample S_1

Fig. 9 FTIR spectrum of CdTe QDs for the sample S_1

4 Conclusions

In summary, highly fluorescent and crystalline MSA capped CdTe QDs in a size and phase tunable mode are successfully synthesized by using a sonication induced modified wet chemical approach. The average sizes of the QDs, estimated from HRTEM images, were able to be controlled from ~ 5.8 to 8.2 nm by tuning the refluxing time from 1 to 4 h, respectively. The estimated average particle sizes by using the Brus equation support the results obtained from HRTEM observation. The bathochromic shift ~ 51 nm of the FL emission peaks of the QDs with the increase of refluxing time also supports the increase in size of the QDs. And also, improvement in crystallinity of the QDs with the increase of refluxing time is confirmed from the enhancement of FL emission intensity of the QDs. CdTe QDs exhibit excitation-dependent FL behaviour. Due to excellent FL properties, MSA capped CdTe QDs can be used for fluorescent labeling, bio-sensing, and biological imaging. The change in defect states on the surface of the QDs with the refluxing time is suggested by the estimated optical constants viz. optical band gap and Urbach energy. The perfomance of size-dependent optical properties of the MSA capped CdTe QDs can lead to development of ratiometric FL probes for detection of metal-ions. From HRTEM images and SAED patterns analysis it was identified that the CdTe QDs possessed a crystalline structure of hexagonal phase and an apparent phase transformation from hexagonal to cubic with the increase of refluxing time. In this sonication induced modified wet chemical approach, QDs are able to be synthesized by changing the refluxing time at constant temperature ~ 100 °C. In addition to that, this sonication induced modified wet chemical approach can also control several desired physical properties of QDs by fine-tuning other synthesis parameters viz. sonication frequency, sonication bath temperature, and sonication duration.

Author contributions DJB and DS contributed to the study concept and design. Material preparation was performed by DJB and DS. DJB contributed to data curation, formal analysis, investigation, and writing of the original draft. ATTM and PKS contributed to reviewing and editing of the manuscript. AD contributed to the validation and visualization. All authors read and approved the final manuscript.

Data availability The data that support the findings of this study are available within the article.

Declarations

Competing interests The authors declare that they have no known competing financial interests or personal relationships that could have appeared to influence the work reported in this paper.

References

1. Arivarasan A, Bharathi S, Vijayaraj V, Sasikala G, Jayavel R. Evaluation of reaction parameters dependent optical properties and its photovoltaics performances of CdTe QDs. J Inorg Organomet Polym Mater. 2018. https://doi.org/10.1007/s10904-018-0803-1.
2. Arivarasan A, Ganapthy S, Alsalme A, Alghamdi A, Jayavel R. Structural, optical and photovoltaic properties of co-doped CdTe QDs for quantum dots sensitized solar cells. Superlattices Microstruct. 2015. https://doi.org/10.1016/j.spmi.2015.10.032.
3. Chandramohan S, Sathyamoorthy R, Lalitha S, Senthilarasu S. Structural properties of CdTe thin films on different substrates. Sol Energy Mater Sol Cells. 2006. https://doi.org/10.1016/j.solmat.2005.04.005.
4. Sinha T, Verma L, Khare A. Variations in photovoltaic parameters of CdTe/CdS thin film solar cells by changing the substrate for the deposition of CdS window layer. Appl Phys A. 2020. https://doi.org/10.1007/s00339-020-04058-4.
5. Das SR, Cook JK. Microstructural, optical and electrical studies of sputtered epitaxial CdTe films. Thin Solid Films. 1988. https://doi.org/10.1016/0040-6090(88)90457-9.
6. Hu JZ. A new high pressure phase of CdTe. Solid State Commun. 1987. https://doi.org/10.1016/0038-1098(87)90273-0.
7. Kumar S, Ade M, Nann T. Synthesis and structural metastability of CdTe nanowires. Chem Eur J. 2005. https://doi.org/10.1002/chem.200400585.
8. Ison VV, Rao AR, Dutta V, Kulriya PK, Avasthi DK. Swift heavy ion induced phase transition in CdTe films deposited by spray pyrolysis in presence of electric field. Nucl Instrum Methods Phys Res B. 2009. https://doi.org/10.1016/j.nimb.2009.05.069.
9. Arizpe-Chavez H, Espinoza-Beltran FJ, Ramirez-Bon R, Zelaya-Angel O, Gonzalez-Hernandez J. Cubic to hexagonal phase transition in CdTe polycrystalline thin films by oxygen incorporation. Solid State Commun. 1997. https://doi.org/10.1016/S0038-1098(96)00554-6.
10. Borah DJ, Mostako ATT, Borgogoi AT, Saikia PK, Malakar A. Modified top-down approach for synthesis of molybdenum oxide quantum dots: sonication induced chemical etching of thin films. RSC Adv. 2020. https://doi.org/10.1039/C9RA09773B.
11. Borah DJ, Mostako ATT, Malakar A. Tailoring the crystalline phase and size of the MoO$_3$ quantum dots via sonication induced modified top-down method. J Alloys Compd. 2021. https://doi.org/10.1016/j.jallcom.2021.161870.
12. Gharibshahi E. Simulation, synthesis and optical properties of cadmium telluride (CdTe) semiconductor nanoparticles. Solid State Commun. 2020. https://doi.org/10.1016/j.ssc.2020.114009.
13. Liu J, Shi Z, Yu Y, Yang R, Zuo S. Water-soluble multicolored fluorescent CdTe quantum dots: synthesis and application for fingerprint developing. J Colloid Interface Sci. 2010. https://doi.org/10.1016/j.jcis.2009.10.061.
14. Gutiérrez-Lazos CD, Ortega-López M, Rosendo E, Ortega-Avilés M, Sánchez-Reséndiz V, Hernández-Hernández A, Meléndez-Lira M, Matsumoto-Kuwabara Y, Espinoza-Rivas AM, Pérez-Guzmán MA. Synthesis of CdTe quantum dots in aqueous solution and their optical and structural characterization. Sci Adv Mater. 2012. https://doi.org/10.1166/sam.2012.1326.
15. Zhang H, Wang L, Xiong H, Hu L, Yang B, Li W. Hydrothermal synthesis for high-quality CdTe nanocrystals. Adv Mater. 2003. https://doi.org/10.1002/adma.200305653.
16. Chakraborty S, Gogoi M, Kalita E, Deb P. Multifunctional, high luminescent, biocompatible CdTe quantum dot fluorophores for bioimaging applications. Int J Nanosci. 2011. https://doi.org/10.1142/S0219581X11008459.
17. Rao H, Liu W, Lu Z, Wang Y, Ge H, Zou P, Wang X, He H, Zeng X, Wang Y. Silica-coated carbon dots conjugated to CdTe quantum dots: a ratiometric fluorescent probe for copper(II). Microchim Acta. 2016. https://doi.org/10.1007/s00604-015-1682-6.
18. Ananthakumar S, Jayabalan J, Singh A, Khan S, Babu SM, Chari R. Size dependence of upconversion photoluminescence in MPA capped CdTe quantum dots: existence of upconversion bright point. J Lumin. 2016. https://doi.org/10.1016/j.jlumin.2015.09.019.
19. Ca NX, Hien NT, Loan PN, Tan PM, Thuy UTD, Phan TL, Nguyen QB. Optical and ferromagnetic properties of Ni-doped CdTeSe quantum dots. J Electron Mater. 2019. https://doi.org/10.1007/s11664-019-07017-9.
20. Rasekholghol A, Fazaeli Y, Dehaghi SM, Ashtari P, Kardan M, Feizi S, Matin MS. CdTe quantum dots on gold-198 nano particles: introducing a novel theranostic agent. Radiochim Acta. 2021. https://doi.org/10.1515/ract-2020-0047.
21. Nideep TK, Ramya M, Sony U, Kailasnath M. MSA capped CdTe quantum dots for pH sensing application. Mater Res Express. 2019. https://doi.org/10.1088/2053-1591/ab35a0.
22. Yuan J, Guo W, Yin J, Wang E. Glutathione-capped CdTe quantum dots for the sensitive detection of glucose. Talanta. 2009. https://doi.org/10.1016/j.talanta.2008.10.032.
23. Yu X, Liu J, Zuo S, Yu Y, Cai K, Yang R. Application of mercaptosuccinic acid capped CdTe quantum dots for latent fingermark development. Forensic Sci Int. 2013. https://doi.org/10.1016/j.forsciint.2013.04.027.
24. Ying E, Li D, Guo S, Dong S, Wang J. Synthesis and bio-imaging application of highly luminescent mercaptosuccinic acid-coated CdTe nanocrystals. PLoS ONE. 2008. https://doi.org/10.1371/journal.pone.0002222.
25. Parani S, Bupesh G, Manikandan E, Pandian K, Oluwafemi OS. Facile synthesis of mercaptosuccinic acid-capped CdTe/CdS/ZnS core/double shell quantum dots with improved cell viability on different cancer cells and normal cells. J Nanopart Res. 2016. https://doi.org/10.1007/s11051-016-3663-z.
26. Carvalho MS, Mayrinck C, Raphael E, Bettini J, Ferrari JL, Schiavon MA. The role that electrolytes play in the synthesis of water-soluble CdTe quantum dots prepared at ambient temperature. J Braz Chem Soc. 2017. https://doi.org/10.21577/0103-5053.20160275.
27. Tauc J. Optical properties and electronic structure of amorphous Ge and Si. Mater Res Bull. 1968. https://doi.org/10.1016/0025-5408(68)90023-8.
28. Baruah JM, Narayan J. Surface passivated aqueous mediated synthesis of CdTe QDs: potential nano thin films. Mater Res Express. 2019. https://doi.org/10.1088/2053-1591/ab31c4.
29. Tyrrell EJ, Smith JM. Effective mass modeling of excitons in type-II quantum dot heterostructures. Phy Rev B. 2011. https://doi.org/10.1103/PhysRevB.84.165328.
30. Urbach F. The long-wavelength edge of photographic sensitivity and of the electronic absorption of solids. Phys Rev. 1953. https://doi.org/10.1103/PhysRev.92.1324.

31. Borah DJ, Mostako ATT, Saikia PK, Dutta P. Effect of thickness and post deposition annealing temperature on the structural and optical properties of thermally evaporated molybdenum oxide films. Mater Sci Semicond Process. 2019. https://doi.org/10.1016/j.mssp.2018.12.038.

32. Borah DJ, Mostako ATT. Investigation on dispersion parameters of molybdenum oxide thin films via Wemple-DiDomencio (WDD) single oscillator model. Appl Phys A. 2020. https://doi.org/10.1007/s00339-020-03996-3.

33. Kyobe JW, Khan MD, Kinunda G, Mubofu EB, Revaprasadu N. Synthesis of CdTe quantum dots capped with castor oil using a hot injection solution method. Mater Sci Semicond Process. 2020. https://doi.org/10.1016/j.mssp.2019.104780.

34. Xiao SJ, Zhao XJ, Chu ZJ, Xu H, Liu GQ, Huang CZ, Zhang L. New off-on sensor for captopril sensing based on photoluminescent MoOx quantum dots. ACS Omega. 2017. https://doi.org/10.1021/acsomega.7b00088.

35. Zhang J, Pan Y, Chen Y, Lu H. Plasmonic molybdenum trioxide quantum dots with noble metal-comparable surface enhanced Raman scattering. J Mater Chem C. 2018. https://doi.org/10.1039/C7TC04807F.

36. Feng X, Shang Q, Liu H, Wang H, Wang W, Wang Z. Effect of adenine on the photoluminescence properties and stability of water-soluble CdTe quantum dots. J Phys Chem C. 2009. https://doi.org/10.1021/jp806116m.

37. Sreekanth K, Siddaiah T, Gopal NO, Kumar YM, Ramu C. Optical and electrical conductivity studies of VO^{2+} doped polyvinyl pyrrolidone (PVP) polymer electrolytes. J Sci Adv Mater Devices. 2019. https://doi.org/10.1016/j.jsamd.2019.06.002.